Hindered rotation of an OH-Li center in MgO: Infrared absorption experiments and theory

Kevin R. Martin,[1,2] Chao Peng,[1] Suppawan Kleekajai,[1] Philip Blaney,[1] Eric Diamond,[1,2] W. Beall Fowler,[1] Michael Stavola,[1] and Roberto González[3]

[1]*Department of Physics and Sherman Fairchild Laboratory, Lehigh University, Bethlehem, Pennsylvania 18015, USA*

[2]*Department of Physics, University of Pittsburgh at Johnstown, Johnstown, Pennsylvania 15904, USA*

[3]*Departamento de Física, Escuela Politécnica Superior, Universidad Carlos III, Avenida de la Universidad, 30, Leganés, 28911 Madrid, Spain*

(Received 27 February 2007; published 18 June 2007)

The infrared absorption spectra of MgO doped with Li and either H or D contain unusually broad absorption bands associated with O-H or O-D stretching vibrations. We have measured the infrared absorption of these bands at low temperatures and find that they can be resolved into distinct components, particularly for the spectrum of O-D. Density-functional-theory calculations show that in equilibrium, the H or D is displaced from the O-Li axis, suggesting the coupling of a hindered rotational degree of freedom with the O-H or O-D stretching mode. We develop a four-well model for this motion by which we analyze the experimental O-D spectra and find excellent agreement with experiment.

DOI: 10.1103/PhysRevB.75.245211 PACS number(s): 61.72.Bb, 63.20.Pw, 78.30.−j

I. INTRODUCTION

Several binary oxides and combinations thereof have become attractive for their potential use as optoelectronic materials.[1–3] Most of the attention has focused on ZnO-based systems, in which one of the added components has been MgO.[4–8] In these systems, hydrogen impurities play an important role,[9–11] often behaving as shallow donors.[12–19]

We have recently studied an OH-Li defect in ZnO,[20,21] combining IR spectroscopy and theory to establish a structural model and to study the vibrational coupling that leads to the temperature-dependent linewidth and shift of the O-H IR absorption. MgO doped with Li also contains OH-Li centers. In this case, there is an unusually broad O-H stretching vibrational band[22,23] with frequency 3430 cm^{-1} at room temperature. The corresponding O-D band lies at 2553 cm^{-1}. The room-temperature widths [full widths at half maximum (FWHMs)] of these bands are approximately 200 and 60 cm^{-1}, respectively. The most common frequencies observed in lithium-free hydrogen-containing crystals have a FWHM of about 10 cm^{-1}. The unusually large widths in Li-doped MgO crystals and their dependence on hydrogen isotope led us to investigate this system further, both experimentally and theoretically. We find that these wide bands, particularly in the case of O-D, are comprised of several overlapping lines with characteristic temperature dependences. We show that these properties are consistent with hindered rotation of a H or D, displaced from the z axis defined by an O and an adjacent Li, and moving in an x-y plane.

II. EXPERIMENTAL PROCEDURE

Single crystals of MgO doped with Li were grown at Oak Ridge National Laboratory by an arc-fusion technique.[24] Li doping was performed by mixing 5% Li_2CO_3 powder with high-purity MgO powder before crystal growth. The concentration of Li impurities in samples prepared in this way was determined by atomic emission spectrophotometry to be approximately[25] 0.04 at. %. The as-grown crystals are H rich. D was introduced into a few samples of MgO:Li by annealing for 2 h at 1200 °C in sealed quartz ampoules that contained 0.7 atm of D_2 gas.[23]

IR absorption spectra were measured with a Bomem DA3.16 Fourier transform spectrometer equipped with a KBr beam splitter and an InSb detector. For measurements made at temperatures above 15 K, samples were cooled in a variable-temperature, cold-finger cryostat. The sample temperature was measured with a chromel-Au:0.07 at. % Fe thermocouple that was attached to the sample holder at a position a few millimeters from the sample. For measurements made at temperatures below 15 K, samples were cooled in an Oxford CF 1204 cryostat using He contact gas. In this case, the temperature was measured with a RhFe resistance sensor mounted on the heat exchanger of the cryostat.

III. EXPERIMENTAL RESULTS

The IR spectra in Fig. 1 show O-H and O-D vibrational lines for a MgO:Li sample in its as-prepared state and for a piece of the same sample that was annealed at 1200 °C in a D_2 ambient. The primary O-H vibrational line at 3460 cm^{-1} has a FWHM of 41 cm^{-1} at 3.5 K [Fig. 1(a)]. This line is narrowed considerably from its width of 200 cm^{-1} at room temperature[22] but remains remarkably broad for a H local vibrational mode at low temperature. The corresponding O-D band consists of two components at 2565 and 2578 cm^{-1} (3.5 K), each with a FWHM of 11.6 cm^{-1}. Similar to the O-H band, the O-D lines are narrower than observed in IR spectra measured at room temperature.

The O-H spectrum in Fig. 1(a) shows a number of additional features that are weaker in intensity than the dominant band at 3460 cm^{-1}. There are two broad lines at 3223 and 3330 cm^{-1} and sharper lines[26] at 3618 and 3679 cm^{-1}. The corresponding broad O-D lines [Fig. 1(b)] are at 2418 and 2487 cm^{-1} along with sharper lines at 2667 and 2712 cm^{-1}. The 3679 cm^{-1} O-H line and the corresponding 2712 cm^{-1}

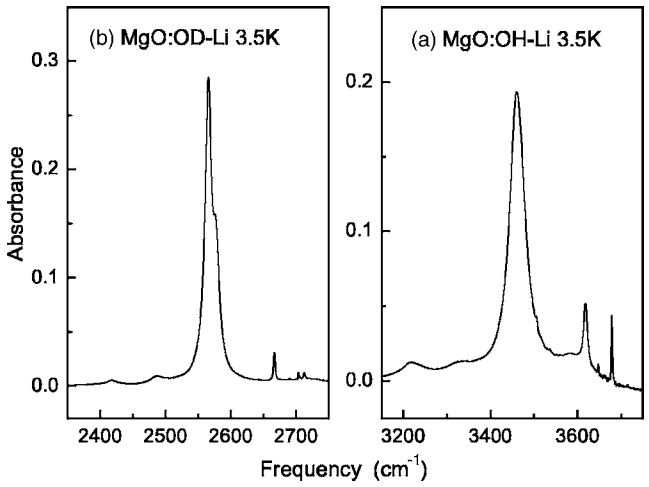

FIG. 1. IR absorption spectra (T=3.5 K, resolution of 1 cm^{-1}) for a MgO crystal doped with Li during growth. The spectrum in (a) is for an as-grown sample that contained hydrogen that was also introduced during growth. The spectrum in (b) is for a sample that was annealed in a D_2 ambient for 2 h at 1200 °C.

O-D line are not seen in every sample, indicating that these lines arise from a defect different from those that give rise to the other lines seen in the O-H and O-D spectra.

Figure 2(a) shows annealing data for the O-D spectrum.

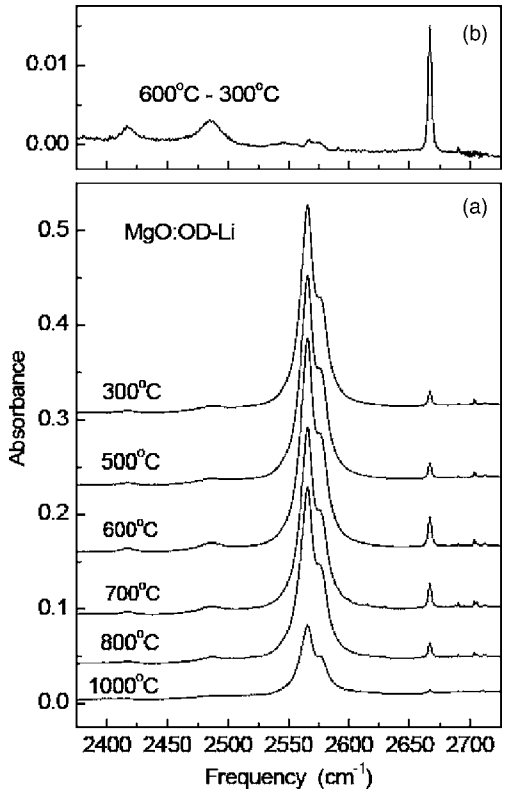

FIG. 2. (a) IR absorption spectra (T=3.5 K, resolution 1 cm^{-1}) for a MgO:Li crystal that was annealed in a D_2 ambient for 2 h at 1200 °C. The sample was annealed sequentially in a He ambient at the temperatures shown prior to measurement at low T. (b) Difference between IR spectra measured following annealing at 600 and 300 °C. (IR spectrum for 600 °C less IR spectrum for 300 °C.)

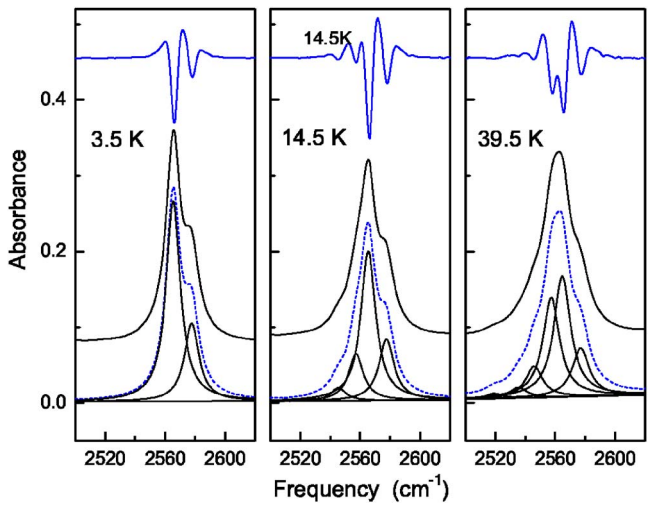

FIG. 3. (Color online) Spectra measured as a function of temperature for the O-D IR band of the OD-Li complex in MgO. The second derivative of the spectrum is shown at the top of each panel (in arbitrary units) just above the measured spectrum. Fits to the data are shown below the measured spectrum.

The strong dominant lines at 2565 and 2578 cm^{-1} anneal away together, consistent with both lines being associated with the same defect. The other lines in the spectrum show a different annealing behavior. The lines at 2418, 2487, and 2667 cm^{-1} increase in intensity upon annealing at 600 °C before they disappear at higher annealing temperatures. This difference in annealing behavior is made apparent by the result shown in Fig. 2(b), where the spectrum measured at 300 °C has been subtracted from the spectrum measured at 600 °C. These results make it clear that the lines at 2418, 2487, and 2667 cm^{-1} are due to defects different from the center that gives rise to the dominant lines at 2565 and 2578 cm^{-1}. Presumably, the situation is similar for the corresponding O-H bands. The focus of the remainder of this paper is on the two dominant O-D lines at 2565 and 2578 cm^{-1} and the corresponding O-H band at 3460 cm^{-1}.

We have examined the temperature dependence of the O-D spectrum. A selection of spectra measured at different temperatures is shown in Fig. 3. At temperatures above 3.5 K, the O-D spectra show additional structure that is characteristic of a number of closely spaced components. The second derivative of each spectrum was evaluated to reveal the additional line components more clearly. Each downward peak in the second derivative spectra shown in Fig. 3 corresponds to a partially resolved IR line component. The positions of the components revealed by the second derivative were used as a starting point for a fit of each IR spectrum with a sum of lines, each with the same Lorentzian width for a given temperature. The results of this fitting procedure are shown in Fig. 3. At 3.5 K, only the lines at 2565 and 2578 cm^{-1} are seen. The relative intensity of these two components is 2.6/1. As the temperature is increased (14.5 K in Fig. 3), two additional lines at 2557 and 2545 cm^{-1} emerge. As the temperature is increased further (39.5 K in Fig. 3), a third pair of lines at 2535 and 2518 cm^{-1} is seen. The transition frequencies for the different components depend only

TABLE I. Experimental (20 K) and four-basis theory frequencies of the line components associated with the O–D stretching band of the OD-Li complex in MgO (in units cm^{-1}).

	ω_1	ω_2	ω_3	ω_4	ω_5	ω_6	ω_7
Experiment	2577.4	2565.2	2557.1	2545.0	2535.0	2518.6	NA
Theory	2577.7	2565.4	2557.9	2545.6	2543.0	2518.6	2582.2

slightly on temperature between 3.5 and 66 K, shifting by less than 1 cm^{-1}. Their values at 20 K are given in Table I. As the temperature is increased, the FWHM of the different line components increases from 11.6 cm^{-1} at 3.5 K to 15 cm^{-1} at 66 K. Above ≈66 K, it becomes difficult to accurately resolve the individual components of the O-D band.

The broader O-H band at 3460 cm^{-1} shows only hints of the rich line structure seen for O-D. The O-H IR band and its second derivative are shown in Fig. 4. In this case, the second derivative shows a dominant peak with a poorly resolved shoulder at higher frequency. By using the results for MgO:Li:OD as a guide, a fit has been made to the O-H band measured at 3.5 K with two components whose relative intensities were constrained to match the relative intensities of the two components at 2565 and 2578 cm^{-1} seen for O-D. A good fit to the 3460 cm^{-1} line shape was obtained with two Lorentzian components with positions 3458 and 3472 cm^{-1}, each with FWHM of 35.4 cm^{-1}, and relative intensities $I(3458)/I(3472)=2.6$. The ratio of the frequencies of corresponding O-H and O-D components is $\omega_{OH}/\omega_{OD}=1.348$, which is consistent with H or D being bonded to a light element such as O. While the fit to the O-H line shape is very good, the absence of clearly resolved structure causes the parameters of the fit to be more dependent on the constraints of the fitting procedure than was the case for the corresponding O-D line shape. The widths of the O-H line components prevent the rich line structure seen for O-D at temperatures higher than 3.5 K from being resolved.

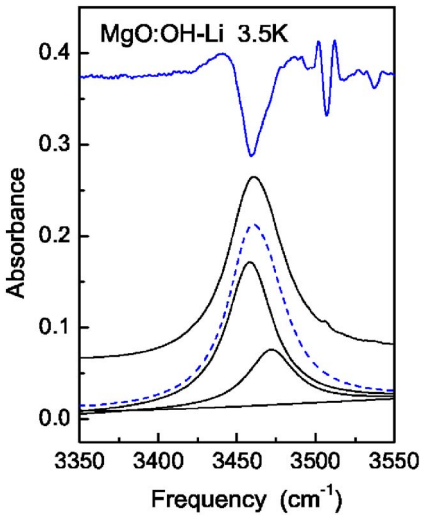

FIG. 4. (Color online) Spectrum (3.5 K) measured for the O-H IR band of the OH-Li complex in MgO. The second derivative of the spectrum (in arbitrary units) is shown above the measured spectrum. A fit to the data is shown below the measured spectrum.

IV. THEORETICAL MODEL

A. Density-functional-theory calculations

We have used CRYSTAL2003 to obtain minimum energies and to map out potential-energy surfaces for the OH-Li defect. CRYSTAL2003 is a recent version of the CRYSTAL family of *ab initio* codes for electronic structure calculations.[27] It utilizes Gaussian basis functions and provides many options, including the choice of basis set and the choice of method [Hartree-Fock or density-functional theory (DFT)]. CRYSTAL2003 also allows automatic geometry optimization.

Given the many choices available for carrying out these calculations, some care must be used in interpreting the computed results. CRYSTAL has, however, been used extensively and its results in general correspond well with those obtained with other methods. Our approach is to combine the results of these *ab initio* calculations with those of simpler models and of experiment to provide insight into the physics of the system.

The computations reported here were carried out with the CRYSTAL2003 code using DFT with a gradient-corrected approximation to the exchange-correlation functional (Becke exchange[28] with 20% Hartree-Fock, Lee-Yang-Parr correlation,[29] 90% nonlocal exchange, 81% nonlocal correlation; potential B3LYP). The calculations were carried out in a periodic supercell approach with one Li substituted for Mg and an adjacent interstitial H impurity in cubic supercells containing 33 atoms. A computed lattice constant of 4.206 Å (which is within 0.25% of the experimental value) was used in all calculations. A $4\times4\times4$ k-point mesh of Monkhorst-Pack[30] type was used. The self-consistent-field energy convergence criterion was 10^{-7} hartree. Gaussian basis functions[31] were of the type $s(3)s(1)s(1)p(1)$ for hydrogen, $s(6)sp(1)sp(1)$ for lithium, $s(8)sp(5)sp(1)$ for oxygen, and $s(8)sp(6)sp(1)$ for magnesium.

After investigating several starting regions for the interstitial H and allowing all atoms to relax in minimizing the energy, we found that in the lowest-energy configuration the H is attached to an O atom and lies in an off-bond-centered site with respect to the O-Li axis, as shown in Fig. 5. That is, if the O atom is initially at (0, 0, 0) and the Li is at (0,0, −2.103) Å, the equilibrium position of the H is at (0.314,0.314,−0.855) Å. Furthermore, there is little relaxation of most of the other atoms except for the Li, which relaxes to (−0.130,−0.130,−2.450) Å; even the O to which the H is attached relaxes only to (0,0,0.012) Å. (A 65-atom supercell calculation predicts identical relaxations to within 1%, as does the use of a larger basis set for Mg and O.)

It is not surprising that we find as well that the Mulliken charges on the atoms are consistent with an ionic picture of MgO: the Mg atoms are approximately Mg^{2+}, most of the

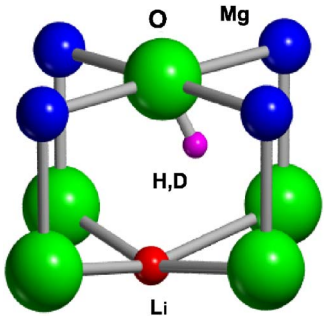

FIG. 5. (Color online) Structure of the MgO:Li:OH defect as predicted by CRYSTAL2003 calculations.

oxygens are O^{2-}, lithium is Li^{+}, and OH is $(OH)^{-}$. It is primarily the ionic repulsion between H and Li that leads to their predicted off-axis configuration.

For this configuration and because of the symmetry of the lattice, there will be four equivalent minima about the z axis—that is, four potential wells within or among which the system can move. Similar configurations will exist with respect to the additional five nearest-neighbor oxygens; however, the O-H bond would have to be broken for the hydrogen to move to one of these, so we analyzed the motion only for the configuration indicated here.

While the H is displaced from the z axis in a (1, 1, 0) direction, the Li is likewise displaced in a $(-1,-1,0)$ direction. Thus, we expect that the rotational motion of the H about the z axis will be accompanied by the motion of the Li. We have carried out point-by-point calculations to find the potential-energy surface in terms of θ, the angle that O-H makes with the z axis, and ϕ, the angle in an x-y plane with respect to the equilibrium position. We find that the force constant for motion in the θ direction is considerably greater than that for motion in the ϕ direction, so we include all of ϕ space but only a small region of θ space in the fit.[32] This process yields

$$V(\theta,\phi) = -3683 + 8065\theta^2 + 4903.5\exp(-4.288\theta^2) + (12.63 + 1791\theta^2)\sin^2(2\phi), \quad (1)$$

with θ and ϕ in radians and $V(\theta,\phi)$ in cm^{-1}. This expression describes four potential wells in an x-y plane, each of which is 413 cm^{-1} from minimum to maximum [$\phi=0$ corresponds to the (110) direction]. The value of θ at equilibrium is 27.1°. As noted above, while the exact numerical results are subject to modification depending on choices made in the calculation, the notion that the H is substantially off the z axis and may be subject to hindered rotation or tunneling in an x-y plane emerges from these results and will be explored in detail in the following section.

B. Four-basis model

The *ab initio* calculations suggest that in addition to the stretching vibration of the O-H and O-D, there is a "channel" around the z axis (at approximately $\theta=30°$) through which the defect system can move, thus another degree of freedom. If there were no ϕ dependence in this channel, the motion would be rotational through the channel, around the z axis. As the four ϕ-dependent wells become deeper, the motion becomes hindered rotation, tunneling, and finally in an extreme limit, libration within each deep well. The differences in the experimental transition energies of the rich line structure of O-D (in the range of 8–20 cm^{-1}) coupled with the calculated depth of the four wells in the channel (413 cm^{-1}) suggest that the motion is within the hindered-rotation–tunneling regime of possible motions through the channel.

We develop and extend here a model similar to that used previously for different systems.[33–35] We use a small basis set of functions and parametrize the Hamiltonian matrix for the hindered-rotation–tunneling motion. The structure of this treatment is independent of whether the motion involves only H or D with Li on axis or a correlated motion of H or D with an off-axis Li. Which choice is better will be discussed later when numerical parameters are obtained from the fit of the model to experiment.

The symmetry of the problem is C_{4v}. We assume that the four wells are deep enough so that we can represent the wave functions by linear combinations of identical basis functions, labeled $|1\rangle$, $|2\rangle$, $|3\rangle$, and $|4\rangle$, centered on each well, which are at some angle θ from the z axis. The coordinate system is defined such that $|1\rangle$, $|2\rangle$, $|3\rangle$, and $|4\rangle$ project into the $(+x)$, $(+y)$, $(-x)$, and $(-y)$ directions, respectively, each representing one of the computed (110) wells. We assume that these four basis functions are normalized, but we will not assume that their overlap is zero. A nonzero overlap arises because the wells may not be deep enough for the basis functions to be totally isolated from each other. The Hamiltonian matrix in this basis must have the form

$$\langle i|H|j\rangle = \begin{pmatrix} E_0 & -t & t' & -t \\ -t & E_0 & -t & t' \\ t' & -t & E_0 & -t \\ -t & t' & -t & E_0 \end{pmatrix}, \quad (2)$$

where E_0 is the intrawell energy, $-t$ is the interwell energy of adjacent wells in the channel, and t' is the interwell energy of opposite wells in the channel. If the system is tunneling, the t parameters will be a measure of the rate of tunneling between the wells.

The overlap matrix in this basis has a similar form and is given by

$$\langle i|j\rangle = \begin{pmatrix} 1 & S & S' & S \\ S & 1 & S & S' \\ S' & S & 1 & S \\ S & S' & S & 1 \end{pmatrix}, \quad (3)$$

where S and S' are the overlap (i.e., the matrix element of the basis functions) between adjacent basis functions and opposite basis functions, respectively, in the channel. Because of the strong potential in θ suggested by our *ab initio* calculations, we expect both t' and S' to be small compared to t and S, respectively.

We wish to find linear combinations of the basis functions that will diagonalize the Hamiltonian and overlap matrices. Using the character table for the group C_{4v}, we find that the

basis vectors decompose into the irreducible representations[36] A_1, E, and B. That is, there will be three energy levels, two nondegenerate and one doubly degenerate. The four linear combinations that will produce wave functions that transform as these irreducible representations are

$$|A_1\rangle = \frac{1}{2\sqrt{1+2S+S'}}(|1\rangle + |2\rangle + |3\rangle + |4\rangle),$$

$$|E^{(1)}\rangle = \frac{1}{\sqrt{2(1-S')}}(|1\rangle - |3\rangle),$$

$$|E^{(2)}\rangle = \frac{1}{\sqrt{2(1-S')}}(|2\rangle - |4\rangle),$$

$$|B\rangle = \frac{1}{2\sqrt{1-2S+S'}}(|1\rangle + |3\rangle - |2\rangle - |4\rangle). \quad (4)$$

These functions are orthonormal, and because there are no off-diagonal Hamiltonian matrix elements in this basis, the energy levels are readily determined. The energy levels are then found to be

$$E(A_1) = \frac{E_0 - 2t + t'}{1+2S+S'},$$

$$E(E) = \frac{E_0 - t'}{1-S'},$$

$$E(B) = \frac{E_0 + 2t + t'}{1-2S+S'}. \quad (5)$$

This hindered-rotational–tunneling-motion energy-level structure will exist in both the $n=0$ and $n=1$ vibrational levels (see Fig. 6), thus giving a "fine structure" to the vibrational transition. To simplify the fit to experiment, we make the following assumptions. (1) The potential energy contained within the Hamiltonian will be shifted, since the zero is arbitrary, such that $E_0=0$. (2) The wells are deep enough so that S' and t' are negligible and thus set to zero. (3) The overlaps S of the hindered-rotation–tunneling wave functions are the same in both the $n=0$ and $n=1$ vibrational states. However, we allow the parameter t to depend on n, the quantum number of the vibration. The parameter for the $n=1$ vibrational state is labeled u, while we retain t for $n=0$.

There are seven transitions allowed by the symmetry between the lower and upper manifolds ($n=0$ and $n=1$). For a single defect, we can separate these transitions into two types. First, if the light is polarized along the symmetry axis of the channel (denoted the z axis), the dipole matrix operator will be proportional to z, which transforms as A_1 in C_{4v}. Thus, for z polarization the allowed transitions are

$$|0A_1\rangle \rightarrow |1A_1\rangle,$$

$$|0E\rangle \rightarrow |1E\rangle,$$

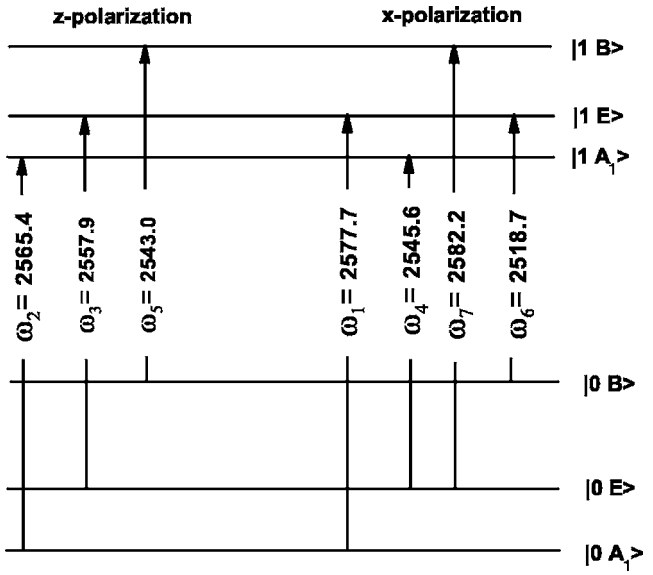

FIG. 6. Theoretical energy-level diagram using the four-basis model, with $S=0.164$, $t=13.2$ cm^{-1}, and $u=8.17$ cm^{-1}, for O-D in MgO:Li. The lower manifold of three levels corresponds to the $n=0$ vibrational level of O-D and the upper manifold to the $n=1$ vibrational level of O-D. The labeling corresponds to that of Table I.

$$|0B\rangle \rightarrow |1B\rangle. \quad (6)$$

The first number is the quantum number of the vibrational state, while the second label denotes the hindered-rotation–tunneling state. In molecular physics language, these would be analogous to the Q branch.[37] The second set of transitions comes from light polarized along the x (or equivalently y) direction. The dipole operator in this case transforms as E in C_{4v}. The allowed transitions will then be

$$|0A_1\rangle \rightarrow |1E\rangle,$$

$$|0E\rangle \rightarrow |1A_1\rangle,$$

$$|0E\rangle \rightarrow |1B\rangle,$$

$$|0B\rangle \rightarrow |1E\rangle. \quad (7)$$

These are analogous to the P and R branches.[37]

With the assumptions stated above, the two energy-level differences in the $n=0$ vibrational manifold are

$$\Delta E(A_1 \leftrightarrow E) = \frac{2t}{1+2S},$$

$$\Delta E(A_1 \leftrightarrow B) = \frac{4t}{(1+2S)(1-2S)}, \quad (8)$$

and likewise for the $n=1$ vibrational manifold,

$$\Delta E(A_1 \leftrightarrow E) = \frac{2u}{1+2S},$$

$$\Delta E(A_1 \leftrightarrow B) = \frac{4u}{(1+2S)(1-2S)}. \tag{9}$$

Thus, there are three parameters to fit within the model with the assumptions that have been made.

The temperature dependence of the experimental lines at 2565 and 2578 cm^{-1} (Fig. 3) indicates that both these lines originate from the ground state of the system. In the model we have developed, there are two such transitions. Thus, the difference in energy between these two transitions must be assigned to $\Delta E(A_1 \rightarrow E)$ in the upper manifold. Likewise, the lines that emerge near 2557 and 2545 cm^{-1} at higher temperature must be consistent within the model as originating from the first excited state in the ground-state manifold, and the lines near 2535 and 2519 cm^{-1} that appear at even higher temperature must be consistent within the model as originating from the second excited state in the ground-state manifold.

Using the experimental frequencies of the lines near 2565, 2578, 2545, and 2519 cm^{-1}, we can uniquely determine the values of S, t, and u by using Eqs. (8) and one of Eqs. (9). Thus, we have

$$\frac{2u}{1+2S} = 12.3\ cm^{-1},$$

$$\frac{2t}{1+2S} = 19.8\ cm^{-1},$$

$$\frac{4t}{(1+2S)(1-2S)} = 59.0\ cm^{-1}. \tag{10}$$

The latter two equations give $S=0.164$ and $t=13.2$ cm^{-1}. Using these values in the first, we find $u=8.17$ cm^{-1}. The six known experimental lines are compared with their theoretical counterparts in Table I. The results determined from the four-basis model yield the energy-level diagram that is shown in Fig. 6. The fit to experiment is remarkably good considering the simplicity of the model and the assumptions that have been made. In addition, the values of the three parameters are quite reasonable. An overlap of about 16% is consistent with assuming that the wells are deep enough that we can approximate the system by only four basis functions. There is a seventh transition predicted near 2582 cm^{-1} that was not identified in the measured spectra.

This four-basis model also gives quantitative predictions for the strengths of all seven predicted transitions. For z polarization, an operator that transforms as A_1 in C_{4v} symmetry (since z transforms in this fashion) can be constructed from the four basis functions. As such,

$$z_{op} = \beta(|1\rangle\langle 1| + |2\rangle\langle 2| + |3\rangle\langle 3| + |4\rangle\langle 4|), \tag{11}$$

and likewise for x polarization,

$$x_{op} = \alpha(|1\rangle\langle 1| - |3\rangle\langle 3|). \tag{12}$$

Making the simplifying assumption that the hindered-rotation-tunneling wave functions are the same in both the $n=0$ and $n=1$ vibrational states, we find the following matrix elements of z_{op} and x_{op}:

$$\langle A_1|z_{op}|A_1\rangle = \beta(1+2S+S'),$$

$$\langle E^{(1)}|z_{op}|E^{(1)}\rangle = \langle E^{(2)}|z_{op}|E^{(2)}\rangle = \beta(1-S'),$$

$$\langle E^{(1)}|z_{op}|E^{(2)}\rangle = 0,$$

$$\langle B|z_{op}|B\rangle = \beta(1-2S+S') \tag{13}$$

and

$$\langle A_1|x_{op}|E^{(1)}\rangle = \frac{\alpha}{\sqrt{2}}\sqrt{1+2S+S'}\sqrt{1-S'},$$

$$\langle A_1|x_{op}|E^{(2)}\rangle = 0,$$

$$\langle E^{(1)}|x_{op}|B\rangle = \frac{\alpha}{\sqrt{2}}\sqrt{1-2S+S'}\sqrt{1-S'},$$

$$\langle E^{(2)}|x_{op}|B\rangle = 0. \tag{14}$$

The transition strengths for a single defect will be proportional to the squares of these matrix elements. To eliminate a proportionality constant, we determine the transition strengths relative to the $A_1(n=0) \rightarrow A_1(n=1)$ transition, i.e., the ratios of the squares of the above matrix elements to the square of the A_1 to A_1 expression. Also, since the experimental spectrum is composed of transitions from an ensemble of defects oriented along the different crystal axes exposed to unpolarized light, we must properly sum over these orientations. The propagation vector of the light is along one of the crystal axes, labeled z. So for z, x, and y oriented channels, the intensity ratio of z transitions (as in Fig. 6) to transitions perpendicular to z will be 0:2, 1:1, and 1:1, respectively. The total spectrum thus will be composed of z to (x,y) transitions in the ratio 2:4, so that the x transition strengths above must be multiplied by 2 relative to z.

Finally, all seven transitions are predicted in the four-basis model to have relative strengths as a function of temperature, with $S=0.164$ and $S'=0$, of

$$\frac{I(2519)}{I(2565)} = 0.381\left(\frac{\alpha}{\beta}\right)^2 \exp\left(\frac{-59.0\ cm^{-1}}{kT}\right),$$

$$\frac{I(2543)}{I(2565)} = 0.256 \exp\left(\frac{-59.0\ cm^{-1}}{kT}\right),$$

$$\frac{I(2546)}{I(2565)} = 0.753\left(\frac{\alpha}{\beta}\right)^2 \exp\left(\frac{-19.8\ cm^{-1}}{kT}\right),$$

$$\frac{I(2558)}{I(2565)} = 1.134 \exp\left(\frac{-19.8\ cm^{-1}}{kT}\right),$$

$$\frac{I(2565)}{I(2565)} \equiv 1,$$

$$\frac{I(2578)}{I(2565)} = 0.753\left(\frac{\alpha}{\beta}\right)^2,$$

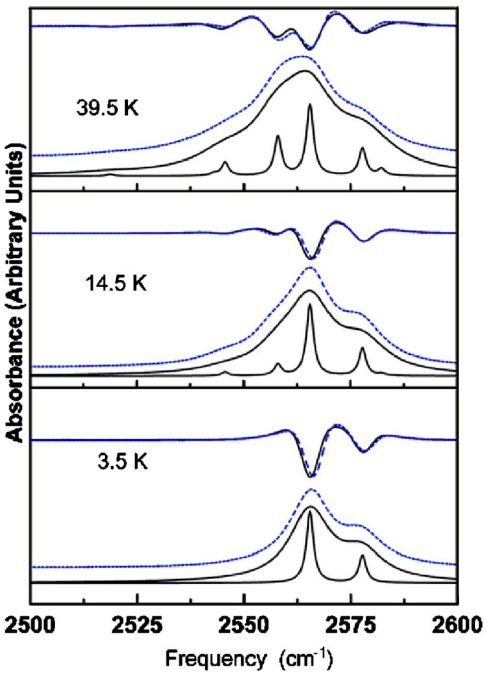

FIG. 7. (Color online) Theoretical and experimental spectra and second derivatives for the O-D vibrational bands of MgO:Li at 4.5, 14.5, and 39.5 K. Theoretical results are shown with solid lines and experimental results are shown with dashed lines. In a given panel, the two lowest plots show spectra calculated from our four-well model, one with FWHM of 2 cm^{-1} and the other with the experimentally determined value (11.6, 12.6, and 14.5 cm^{-1} for temperatures of 3.5, 14.5, and 39.5 K, respectively). All theoretical spectra are normalized so that the peak value near 2565 cm^{-1} is one. The next higher curve is the experimental spectrum, displaced upward for comparison and rescaled so that the peak to asymptote is approximately the same as the theoretical spectrum. Theoretical and experimental second derivatives at the top of each panel are superimposed and rescaled so that their minima near 2565 cm^{-1} are equal.

$$\frac{I(2582)}{I(2565)} = 0.381\left(\frac{\alpha}{\beta}\right)^2 \exp\left(\frac{-19.8\ \mathrm{cm}^{-1}}{kT}\right). \qquad (15)$$

Only one new parameter has been introduced, α/β, which can be determined from the experimental ratio of the intensity of the 2578 cm^{-1} line to the 2565 cm^{-1} line. This experimental ratio is 0.385. This gives the ratio[38] $\alpha/\beta=0.715$.

Figure 7 shows a plot of the predicted and experimental spectra, as well as the predicted and experimental second derivatives of the spectra. For the theoretical spectrum, all transitions are assumed Lorentzian shaped, with the same FWHM. In order to clearly see all seven predicted transitions and their temperature dependence, we plot the theoretical spectrum with a FWHM of 2 cm^{-1} at the lowest part of the plot. For comparison to experiment, we use FWHM values of 11.6, 12.0, and 14.5 cm^{-1} for temperatures of 3.5, 14.5, and 39.5 K, respectively. These values for the theoretical FWHM are identical to the extracted experimental values. The consistency with experiment is remarkable, given the simplifications assumed for the values of the parameters, as well as by the small number of basis functions assumed. The predicted intensity of the 2582 cm^{-1} transition, not uncovered in the measured spectra, is very weak and may be unresolved from the stronger 2578 cm^{-1} transition. The theoretical second derivative of the spectrum shown in Fig. 7 does not show any hint of the presence of the 2582 cm^{-1} line, consistent with experiment.[39]

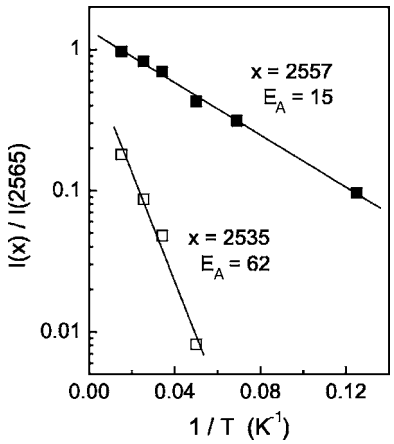

FIG. 8. Plots of $\ln[I(2557)/I(2565)]$ and $\ln[I(2535)/I(2565)]$ vs $1/T$ for the components of the O-D IR band of the OD-Li complex in MgO. The lines are the results of least-squares fits to the data and yield the activation energies shown. Line frequencies and activation energies have units of cm^{-1}.

The predicted 2543 cm^{-1} transition frequency varies somewhat from the experimentally observed 2535 cm^{-1} line frequency. However, given the simplifications of the theory and the uncertainty in fitting the Lorentzians to the experimental data, we deem this discrepancy to not be significant. Indeed, if we relax the assumption that the overlap S is the same in both the $n=0$ and $n=1$ vibrational states, a better fit can be obtained. We do not see a reason to complicate our model, because the analysis at this point strongly suggests that the rich structure seen in the O-D system is due to a hindered-rotation–tunneling motion.

The level scheme shown in Fig. 6 predicts a temperature dependence for the relative intensities of the components of the MgO:Li:OD band that can be compared with the experimental intensities determined from the fits to the IR line shapes discussed in Sec. III. We consider the intensities of the stronger of the lines that originate from the manifold of levels associated with the ground vibrational state. The natural logarithm of the ratio of the area of the 2557 cm^{-1} line that originates from the first excited state to the area of the 2565 cm^{-1} line that originates from the ground state, i.e., $\ln[I(2557)/I(2565)]$, is plotted vs T^{-1} in Fig. 8. Similarly, the area of the 2535 cm^{-1} line that originates from the second excited level of the ground vibrational manifold is considered, and $\ln[I(2535)/I(2565)]$ vs T^{-1} is also plotted in Fig. 8. The slopes of the fits to these plots yield Boltzmann energies of 15 and 62 cm^{-1}. These values can be compared with the values determined from the fit of our model to the experimental transition energies, 19.8 and 59.0 cm^{-1} [see Eq. (10)]. The accuracies of the Boltzmann energies are limited by the accuracy of the measurements of the sample temperature at

low T and the assumptions made in the fitting procedure for the O-D line shapes, e.g., that all components have the same width at a given temperature. The level energies, determined from the small differences between the O-D stretching energies, are also subject to an error of a few cm^{-1}. Therefore, the agreement of the Boltzmann energies with the energies of the levels of the ground-state manifold determined from the transition energies is considered to be very good.

We finally return to the possibility that Li is involved in the motion. First, it is expected that the H or D will remain within the vicinity of the Li^+ ion to maintain a net +2 charge in the region, as would be present if the Mg were at the lattice site. But the H or D will also repel the Li^+ due to the Coulomb interaction. This is consistent with the *ab initio* calculations of Sec. IV A which indicate that the Li relaxes away from the H or D. Thus, it is likely that if the Li is involved in the motion, it will exhibit a motion that is correlated with that of the H or D, attempting to avoid the H or D as they rotate around the z axis. That means the symmetry will still be C_{4v}, and the four-basis model will still be applicable in its current formulation.

Furthermore, another point of view may be helpful in this case. We have expanded the analytical potential in Eq. (1) derived from the *ab initio* calculations in terms of spherical harmonics up to and including $L=8$. We then considered a three-dimensional rotation subject to this potential. While we have not analyzed the experimental data in detail using this model, we have found that order-of-magnitude agreement requires that the rotational constant $B=\hbar^2/2I$ must be lower than the value obtained if only the H or D were rotating through the channel. That is, I, the moment of inertia, must be larger than expected. This would be the case if the lithium was involved in the motion. Assuming a bond length of 0.974 Å for O-D, B has a value of ≈ 10 cm^{-1} with no lithium motion involved. Our initial calculations using the spherical harmonic expansion for the potential in Eq. (1) suggest that B has a value in the range of 4–5 cm^{-1}. Further work is needed to more fully investigate these details of the motion.

V. CONCLUSIONS

The OD-Li complex in MgO is a spectroscopically rich system with fascinating microscopic properties. The direct interplay between theory and experiment has enabled us to determine that the O-D vibrational lines associated with this defect at 2565 and 2578 cm^{-1} (3.5 K) and the additional spectroscopic structure that appears at elevated temperatures are due to the hindered-rotation–tunneling of the D atom in a channel around the O-Li axis. A simple four-basis tunneling model has been developed, and the agreement of the predictions of this model with experiment is remarkable. However, there are still unanswered questions. What is the origin of the widths of the component lines, and why are these widths so dependent on H or D isotope? These and other questions about MgO:Li:OD and related defect systems are the subject of ongoing work.

ACKNOWLEDGMENTS

The work performed at Lehigh University was supported by NSF Grant No. DMR 0403641 as well as by the NSF REU program during the summers of 2005 and 2006. The work of K.R.M. was supported, in part, by a grant from the University of Pittsburgh at Johnstown. That author thanks UPJ for its support. Research at the University Carlos III was supported by the DGI of Spain under Contract No. MAT 2005-04365. The authors thank Yok Chen for helpful interactions and for his assistance in providing experimental samples.

[1] S. J. Pearton, D. P. Norton, K. Ip, Y. W. Heo, and T. Steiner, Prog. Mater. Sci. **50**, 293 (2005).
[2] Ü. Özgür, Ya. I. Alivov, C. Liu, A. Teke, M. A. Reshchikov, S. Doğan, V. Avrutin, S.-J. Cho, and H. Morkoç, J. Appl. Phys. **98**, 041301 (2005).
[3] D. C. Look, B. Claflin, Ya. I. Alivov, and S. J. Park, Phys. Status Solidi A **201**, 2203 (2004).
[4] A. Ohtomo, M. Kawasaki, T. Koida, K. Masubuchi, H. Koinuma, Y. Sakurai, Y. Yoshida, T. Yasuda, and Y. Segawa, Appl. Phys. Lett. **72**, 2466 (1998).
[5] T. Gruber, C. Kirchner, R. Kling, F. Reuss, and A. Waag, Appl. Phys. Lett. **84**, 5359 (2004).
[6] Y. W. Heo, C. Abernathy, K. Pruessner, W. Sigmund, D. P. Norton, M. Overberg, F. Ren, and M. F. Chisholm, J. Appl. Phys. **96**, 3424 (2004).
[7] Andrei Malashevich and David Vanderbilt, Phys. Rev. B **75**, 045106 (2007).
[8] R. Ghosh and D. Basak, J. Appl. Phys. **101**, 023507 (2007).
[9] S. J. Jokela and M. D. McCluskey, Phys. Rev. B **72**, 113201 (2005).
[10] D. G. Thomas and J. J. Lander, J. Chem. Phys. **25**, 1136 (1956).
[11] M. G. Wardle, J. P. Goss, and P. R. Briddon, Phys. Rev. Lett. **96**, 205504 (2006).
[12] C. G. Van de Walle, Phys. Rev. Lett. **85**, 1012 (2000); Anderson Janotti and Chris G. Van de Walle, Nat. Mater. **6**, 44 (2007).
[13] S. F. J. Cox, E. A. Davis, S. P. Cottrell, P. J. C. King, J. S. Lord, J. M. Gil, H. V. Alberto, R. C. Vilão, J. Piroto Duarte, N. Ayres de Campos, A. Weidinger, R. L. Lichti, and S. J. C. Irvine, Phys. Rev. Lett. **86**, 2601 (2001).
[14] D. M. Hofmann, A. Hofstaetter, F. Leiter, H. Zhou, F. Henecker, B. K. Meyer, S. B. Orlinskii, J. Schmidt, and P. G. Baranov, Phys. Rev. Lett. **88**, 045504 (2002).
[15] Y. M. Strzhemechny, H. L. Mosbacker, D. C. Look, D. C. Reynolds, C. W. Litton, N. Y. Garces, N. C. Giles, L. E. Halliburton, S. Niki, and L. J. Brillson, Appl. Phys. Lett. **84**, 2545 (2004).
[16] C. H. Seager and S. M. Myers, J. Appl. Phys. **94**, 2888 (2003).
[17] E. V. Lavrov, J. Weber, F. Börrnert, C. G. Van de Walle, and R. Helbig, Phys. Rev. B **66**, 165205 (2002).
[18] M. D. McCluskey, S. J. Jokela, K. K. Zhuravlev, P. J. Simpson, and K. G. Lynn, Appl. Phys. Lett. **81**, 3807 (2002).
[19] G. A. Shi, M. Stavola, S. J. Pearton, M. Thieme, E. V. Lavrov, and J. Weber, Phys. Rev. B **72**, 195211 (2005).

[20] G. A. Shi, M. Stavola, and W. B. Fowler, Phys. Rev. B **73**, 081201(R) (2006).
[21] K. R. Martin, P. Blaney, G. Shi, M. Stavola, and W. B. Fowler, Phys. Rev. B **73**, 235209 (2006).
[22] R. González, Y. Chen, and K. L. Tsang, Phys. Rev. B **26**, 4637 (1982).
[23] R. González, R. Ramírez, M. Tardío, Y. Chen, and M. R. Kokta, Phys. Rev. B **74**, 014102 (2006).
[24] M. M. Abraham, C. T. Butler, and Y. Chen, J. Chem. Phys. **55**, 3752 (1971).
[25] Y. Chen, E. Montesa, J. L. Boldú, and M. M. Abraham, Phys. Rev. B **24**, 5 (1981).
[26] The 3679 cm^{-1} line was seen in earlier studies (Ref. 23) of MgO:Li:OH. A hint of the 3618 cm^{-1} line can also be seen as a weak, poorly resolved shoulder to the primary 3460 cm^{-1} band in room-temperature IR data reported previously.
[27] V. R. Saunders, R. Dovesi, C. Roetti, R. Orlando, C. M. Zicovich-Wilson, N. M. Harrison, K. Doll, B. Civalleri, I. Bush, Ph. D'Arco, M. Llunell, *Crystal2003 User's Manual* (University of Torino, Torino, 2003).
[28] D. Becke, Phys. Rev. A **38**, 3098 (1988).
[29] C. Lee, W. Yang, and R. G. Parr, Phys. Rev. B **37**, 785 (1988).
[30] H. J. Monkhorst and J. D. Pack, Phys. Rev. B **13**, 5188 (1976).
[31] Basis functions were obtained from the web site of M. D. Towler (http://www.tcm.phy.cam.ac.uk/~mdt26/crystal.html) and from R. Krishnan, J. S. Binkley, R. Seeger, and J. A. Pople, J. Chem. Phys. **72**, 650 (1980).
[32] The computed energies were fit to an analytical expression similar to that used by D. R. Bosomworth, W. Hayes, A. R. L. Spray, and G. D. Watkins, Proc. R. Soc. London, Ser. A **317**, 133 (1970) in their treatment of interstitial O in Si.
[33] E. E. Haller, B. Joos, and L. M. Falicov, Phys. Rev. B **21**, 4729 (1980).
[34] Emilio Artacho and L. M. Falicov, Phys. Rev. B **43**, 12507 (1991).
[35] K. R. Martin and W. B. Fowler, Phys. Rev. B **52**, 16516 (1995).
[36] See, for example, M. Tinkham, *Group Theory and Quantum Mechanics* (McGraw-Hill, New York, 1964). Whether the B representation should be B_1 or B_2 depends upon the choice of notation for the two physically different reflection planes containing the z axis. Thus, we simply label it B.
[37] See, for example, G. Herzberg, *Spectra of Diatomic Molecules* (Van Nostrand, New York, 1950), p. 508.
[38] α and β should be proportional to the projection of the dipole operator on the x and z axes, respectively. If we require that x_{op}^2 and y_{op}^2 have identical matrix elements with respect to a vector of C_{4v} symmetry and set $S'=0$, we find $\tan(\theta)=(\alpha/\beta)\sqrt{1/2(1+2S)}$. With $\alpha/\beta=0.715$ and $S=0.164$, this yields $\theta=23.7°$. This compares well with the computed value (Sec. IV A) of 27.1°.
[39] Another possibility for the predicted 2582 cm^{-1} transition is apparent from Figs. 3 and 7, where there is a hint in the experimental second derivative of another line near 2590 cm^{-1} at elevated temperature.